Hindawi
Complexity
Volume 2022, Article ID 2132005, 20 pages
https://doi.org/10.1155/2022/2132005

Research Article

An Optimized Design of New *XYθ* Mobile Positioning Microrobotic Platform for Polishing Robot Application Using Artificial Neural Network and Teaching-Learning Based Optimization

Minh Phung Dang,[1] Hieu Giang Le,[1] Ngoc Le Chau,[2] and Thanh-Phong Dao[3,4]

[1]*Faculty of Mechanical Engineering, Ho Chi Minh City University of Technology and Education, Ho Chi Minh City, Vietnam*
[2]*Faculty of Mechanical Engineering, Industrial University of Ho Chi Minh City, Ho Chi Minh City, Vietnam*
[3]*Division of Computational Mechatronics, Institute for Computational Science, Ton Duc Thang University, Ho Chi Minh City, Vietnam*
[4]*Faculty of Electrical & Electronics Engineering, Ton Duc Thang University, Ho Chi Minh City, Vietnam*

Correspondence should be addressed to Thanh-Phong Dao; daothanhphong@tdtu.edu.vn

Received 13 August 2022; Accepted 6 October 2022; Published 7 November 2022

Academic Editor: Gonzalo Farias

Compliant mechanisms with flexure hinges have been widely applied for positioners, bioengineering, and aerospace. In this study, a new optimized design method for the mobile microrobotic platform was developed for the polishing robot system. A metaheuristic-based machine learning technique in combination with finite element analysis (FEA) was developed. The designed platform allows three degrees of freedom with two x-and-y translations and one z-axis rotation. A new hybrid displacement amplification mechanism was also developed using Scott-Russell and two-lever mechanisms to magnify the workspace of the platform. The leaf hinges were employed due to their large rotation, and the right circular hinges were adopted because of their high accuracy. In modeling the behaviors of the developed platform, the artificial neural network is formulated in combination with the teaching-learning-based optimization (TLBO) method. The ANN architecture was optimized through TLBO to a better approximation. And then, three optimized case studies were conducted by the TLBO. The data is collected through FEA simulation. The modeling results from the TLBO-based ANN were well established with excellent metrics of R, R^2, and MSE. The optimized results found that the proposed MPM platform achieves a max-y stroke of 1568.1 μm, max-x stroke of 735.55 μm, and max-θ rotation angle of 2.26 degrees. The proposed MPM platform can operate at a high displacement amplification ratio of over 9.

1. Introduction

Compliant mechanisms play a vital role in ultrahigh precision engineering, such as stable switch [1, 2], vibration-assisted cutting [3], manipulations/micrograppers [4], fast servo in precision machining, energy harvester [5], alignment of optics [6], robotics [7], and so on. Compared with rigid-link counterparts, compliant mechanisms can propose a high resolution with precise smooth motion due to the excellent advantages such as without backlash, no friction, reduced assembly, cheap manufacture, and monolithic structure.

Currently, many planar compliant mechanisms from one degree of freedom (DOF) to three-DOF motions have been developed by using series architecture, parallel chain, or hybrid series-parallel type. The one DOF mechanisms often have a high accuracy with a minimal parasitic motion, but these mechanisms have still limited in some applications, e.g., positioners [8]. Then, two DOF mechanisms have been designed to propose more complicated applications, i.e., scanner [9]. The two DOF mechanisms possess a decoupled property. Although one or two DOF mechanisms can achieve a wide stroke, simple control, and high accuracy but their applications are still limited. Therefore, three DOF mechanisms have been developed as alternatives for many planar applications as a positioner, manipulation, and so forth [10]. However, the workspace of two translations and one rotation of the existing three DOF mechanisms are still small. To overcome such drawbacks, a kinematic structure with better properties is needed to provide a high load capacity, large stroke, high safety factor, and high stiffness. Hence, three DOF mechanisms have attracted much attention and become a hot topic for researchers.

Generally speaking, complaint mechanisms, which are acted by piezoelectrical actuators (PZT), have limited workspace. To overcome this drawback, many displacement amplification mechanisms were proposed to amplify the stroke of PZTs, such as Scott–Russell mechanism, lever and bridge types [11]. In addition, a lot of other researchers have also designed many different types of three-DOF compliant positioning platforms with desired characteristics. A micropositioning stage with 3-DOF was designed [12]. In this study, the compliance matrix and finite element method were utilized to build the stiffness and the input coupling ratio of the stage. Besides, the parameters of the stage were optimized to minimize the input coupling ratio. A 3-DOF spatial precision manipulation was designed and analyzed [13]. The translational and angular displacements were analyzed in this article. Besides, a 3-DOF translational mechanism was proposed, and it was analyzed via the pseudo-rigid-body model (PRB) method [14]. By using the PRB technique, another 3-DOF mechanism with two translations and one rotation was designed and analyzed [15]. This type for nanopositioning application was analyzed by a compliance matrix [16].

Although the discussed 3-DOF stages have been designed with multiple excellent characteristics, but the structure is still complicated. Moreover, the workspaces are still limited. Considering an application of 3-DOF compliant mechanisms in the robots, a planar micropositioning platform was designed, and the manufacturing error was analyzed [17]. Almost the behavior analysis of the previous stages employed some popular analytical techniques, such as PRB and compliance matrix. With high nonlinear characteristic behavior, modeling of them has a large error. This causes a large manufacturing error, decreasing the practical positioning ability. To overcome this obstacle, a new approach based on machine-learning-based methods and metaheuristics is devoted in the present article. The artificial neural network (ANN) is combined with the teaching-learning-based optimization algorithm (TLBO) in modeling the behaviors of a new $XY\theta$ mobile positioning microrobotic platform. The developed microrobotic platform can basically be applied for vibration-based polishing robot applications.

Motivated by the gaps between the existing studies, this paper presents an optimized design method for a three-DOF mobile microrobotic platform for use in polishing robot application. The developed platform is able to provide a large workspace in the x-and-y translations and rotation around the z-axis. In modeling the behaviors of the proposed microrobotic platform, artificial neural network is adopted to resolve the stroke and safety factor. To overcome the ANN limitations, the TLBO algorithm was extended to optimize the ANN approximate accuracy. Then, the geometrical factors of the proposed microrobotic platform were optimized by adopting the TLBO algorithm. Finally, three case studies are considered to confirm the accuracy and effectiveness of the proposed methodology.

2. Conceptual Design of $XY\theta$ Mobile Positioning Microrobotic Platform

A basic application of the $XY\theta$ mobile positioning microrobotic (MPM) platform is used for manipulations and precise sample positioning from sub-micrometer to hundreds of micrometer scales. Figure 1 illustrates a design scheme of the MPM platform. The proposed MPM platform utilizes three piezoelectric stack actuators (PZT) to actuate an input displacement to three corresponding robotic legs (robotic leg #1, robotic leg #2, and robotic leg #3).

By arranging three robotic legs around a circle with 120 degrees and three PZTs located in a tripedalism, so-called tripedal topology, the MPM platform can generate a locomotion in three DOF on a planar surface. It means that the platform includes three main motions, such as two translations along the x-and-y axes and one rotation (θ_z) around the z-axis.

Overall, the MPM platform was manufactured with a monolithic flexure-based mechanism. The fabrication will be carried out via wire electrical discharged machining (WEDM). Each robotic leg was also a flexure structure that consists of a hybrid displacement amplification mechanism (HDAM) in combination with a leaf hinge. The robotic leg #1 was defined in a local coordinate of $O_1X_1Y_1$. The robotic leg #2 and the robotic leg #3 were defined in a local coordinate of $O_2X_2Y_2$ and $O_3X_3Y_3$, respectively. More details of the HDAM are presented in next section. Under actuating the three PZTs simultaneously, the mobile platform of the microrobot makes two translations δx_1 and δy_1, and a rotation θ_1.

Technical requirements and specifications of the MPM platform in the design phase are expected to achieve large strokes in the translations over 1000 (μm) or higher than 1 mm and a wide rotation. Furthermore, a high safety factor of over 1.8 is required. The mentioned importantly technical specifications of the MPM platform can fulfil the practical applications. In addition, Al 7075-T651 is chosen to manufacture the microrobotic platform. The properties of Al 7075-T651 are listed, including a density of 2810 kg/m^3, Poisson ratio of 0.33, yield stress of 503 MPa, and Young's modulus of 71.7 GPa.

Figure 2 illustrates the assembly scheme of $XY\theta$ mobile positioning microrobotic platform.

As shown in Figure 2, it includes the following key components:

(1) Preload crew,

(2) PZT mounting plate,

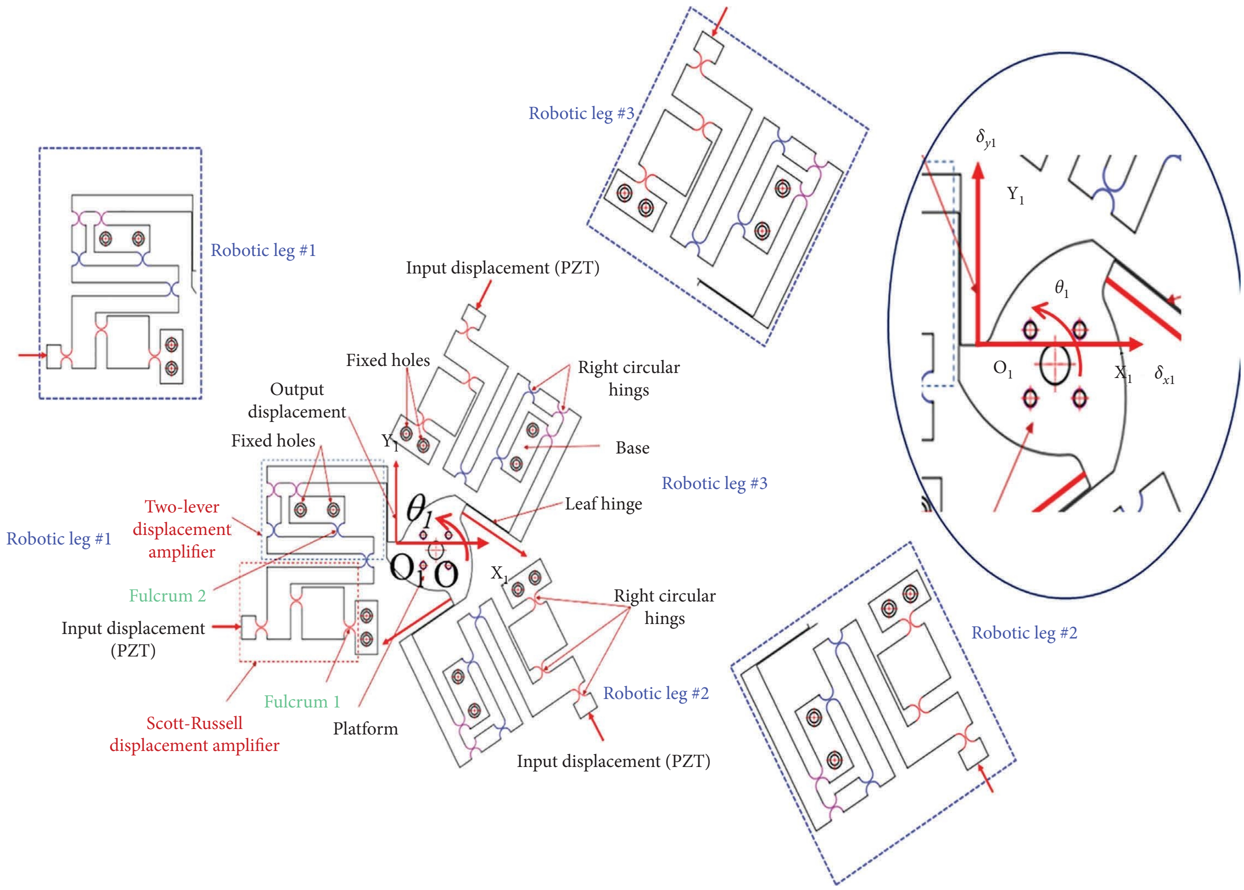

FIGURE 1: Design scheme of $XY\theta$ mobile positioning microrobotic platform.

(3) PZT actuator,

(4) Intermediate plate,

(5) Prototype,

(6) Anti-vibration fixing plate,

(7) Fixed hole.

As depicted in Figure 2, the prototype of the proposed microrobotic platform was mounted on the intermediate plate. The PZTs were fixed on the PZT mounting plate, and the preload screw was employed to adjust the PZT in contact with the input port of the platform. Finally, the whole of the system was put on the anti-vibration table.

A basic application of the proposed MPM platform is able to be employed for polishing robot system, as given in Figure 3. The proposed platform is mounted on the station. The polished sample is located on the mobile platform through fixing screws while the end-effector of the robotic arm brings the polishing tool.

When three PZTs act, the platform causes a micro-vibration for the sample. The micro-vibration is aimed to reduce the friction between the sample and the polishing tool. This leads to improvement of the surface roughness of the final workpiece. This machining process is considered as a vibration-assisted polishing process.

The dimensional scheme of the proposed MPM platform is provided in Figure 4, and the main dimensions are given in Table 1. The thickness of the platform in the out plane (z-axis) is 8 mm.

2.1. Analysis of Hybrid Displacement Amplification Module. Figure 5 provides a new hybrid displacement amplifier. The suggested HDAM is built by a combination of Scott–Russell mechanism (SRM) amplifier with a two-lever displacement (TLD) amplifier. The hybrid amplifier is moved based on the deformation of right circular hinges. In the beginning, an input displacement of 135 μm along the x-axis is acted to the SRM amplifier, and this displacement amplifier is rotated around the fulcrum (1) and then, the output motion of the SRM is transformed to the input port of the TLD amplifier, and this mechanism is rotated about the fulcrum (2) the output displacement is collected along the y-axis. Finally, the output motion of the proposed HDMA is kept to transfer to the leaf hinge (see Figure 1) so that the MPM platform is moved.

To illustrate the amplification ratio of the proposed HDMA, the proposed HDMA is meshed and simulated by finite element analysis (FEA) ANSYS 2019R1 software. The number of nodes and elements are about 29047 and 16867, respectively. The quality of the mesh is measured by the Skewness technique with an average value of 0.44906. The results of the HDMA are provided in Table 2.

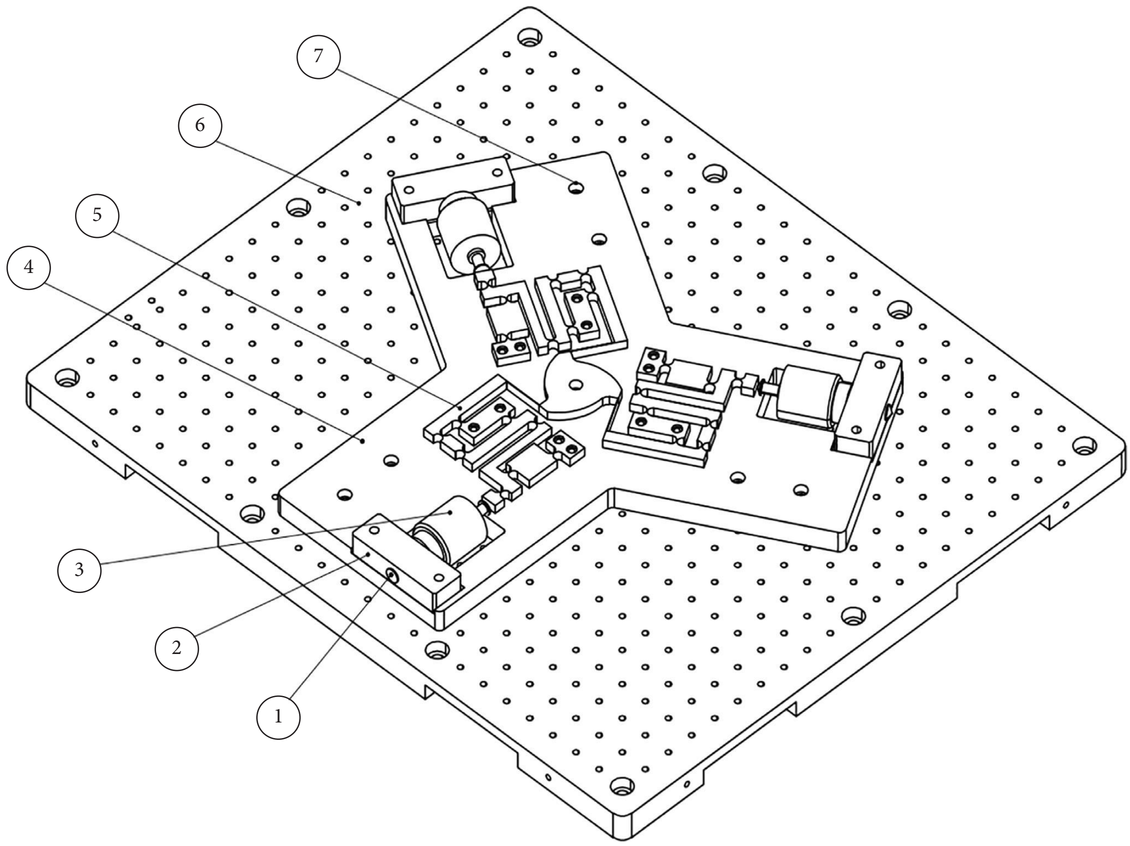

Figure 2: Assembly scheme of $XY\theta$ mobile positioning microrobotic platform: (1) preload crew, (2) PZT mounting plate, (3) PZT actuator, (4) intermediate plate, (5) prototype, (6) anti-vibration fixing plate, (7) fixed hole.

The results of Table 2 indicates that the amplification ratio of the proposed hybrid amplifier is about 12.43 with a high safety factor (SF) over 1.4 when the input displacement is from 90 μm to 145 μm. Besides, the stress is still lower than the yield stress of the material (503 MPa).

2.2. Initial Evaluation of Static and Dynamic Behavior of Microrobotic Platform. In order to evaluate the initial specifications of the proposed MPM platform, the static and dynamic behaviors are simulated by ANSYS software. The three PZTs are employed simultaneously with 135 μm, and the output stroke/displacement of the robotic leg #1 is measured. Figure 6(a) shows the boundary conditions for simulating the platform. The number of nodes is 71202, and the number of elements is 41045. Skewness average value is about 0.4877, as given in Figure 6(b).

Figure 7 depicts the stress concentration. It is found that the high stress appeared on the surfaces of leaf hinges and right circular hinge.

The deformation of the MPM platform is provided in Figure 8.

The initial evaluation showed that the amplification ratio of the proposed MPM platform is about 9.85, with a high safety factor (SF) over 1.7 when the input displacement is from 90 μm to 145 μm. Besides, the stress is still smaller than the yield stress of material (503 MPa), as depicted in Table 3.

The dynamic behavior is achieved by FEA simulations. The four natural frequencies for the first mode shapes include 102.036 Hz, 113.81 Hz, 113.9 Hz, and 154.84 Hz, respectively, as provided in Table 4. Considering a resonance of the proposed MPM platform with the PZTs and others, the first mode shape is a z-axis translation. The second mode shape is the x-axis translation. The third mode shape is the z-axis translation. Finally, the fourth mode shape is the z-axis rotation.

2.3. Formulation of Optimization Problems. The characteristics of the proposed MPM platform are desirable to gain the two main design targets, including a large stroke (δy_1) and a high safety factor.

When the stroke is enhanced, the rotation of the platform (θ_1) is also improved. A good SF over 1.8 can ensure a long working time. Based on the initial evaluations in the previous parts, it determined that the performances of the proposed MPM platform are strongly affected by varying the thickness values of right circular hinges (A, B, C, D) and the thickness of the leaf hinges (E).

Three optimization problems of the proposed MPM platform are considered as follows.

Case #1.: maximize the stroke

Find design variables: $\mathbf{X} = [A, B, C, D, E]$

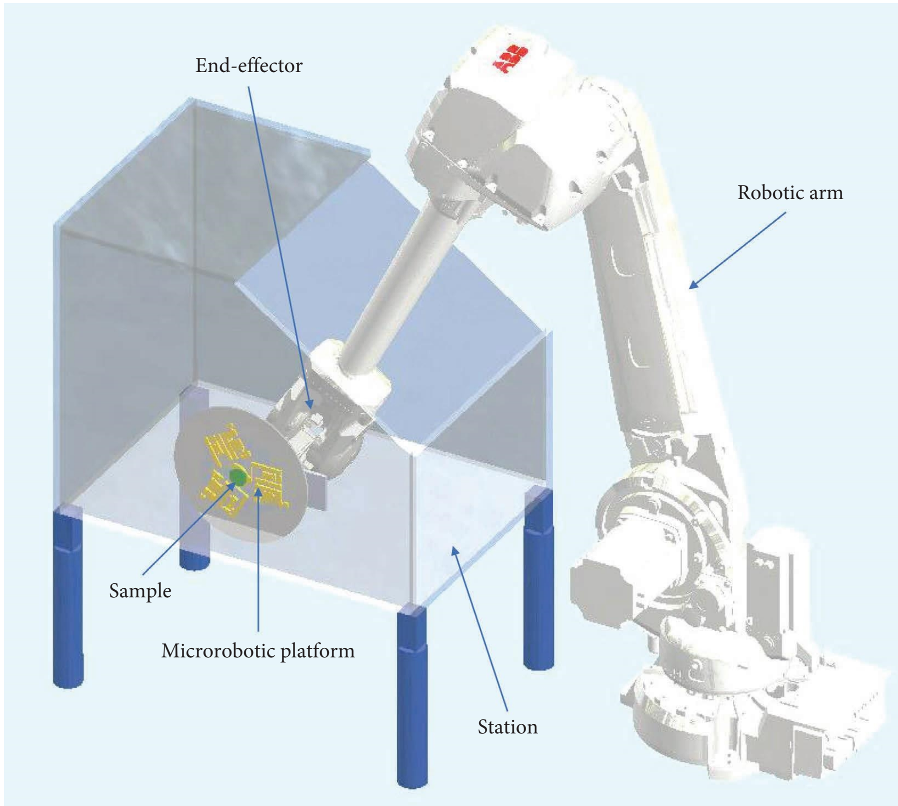

Figure 3: Application of microrobotic platform for polishing.

$$\text{Maximize}: f_1(\mathbf{X}). \quad (1)$$

Bounds of design variables (unit: mm):

$$\begin{cases} 0.8 \le A \le 0.9 \\ 0.7 \le B \le 0.8 \\ 0.6 \le C \le 0.7 \\ 0.55 \le D \le 0.6 \\ 45 \le E \le 50 \end{cases}. \quad (2)$$

Case #2.: maximize the safety factor

Find design variables: $\mathbf{X} = [A, B, C, D, E]$

$$\text{Maximize}: f_2(\mathbf{X}). \quad (3)$$

Bounds of design variables (unit: mm):

$$\begin{cases} 0.8 \le A \le 0.9 \\ 0.7 \le B \le 0.8 \\ 0.6 \le C \le 0.7 \\ 0.55 \le D \le 0.6 \\ 45 \le E \le 50 \end{cases}. \quad (4)$$

Case #3.: maximize the stroke and the safety factor simultaneously (multi-objective optimization problem)

Find design variables: $\mathbf{x} = [A, B, C, D, E]$

$$\begin{cases} \text{Maximize}: f_1(\mathbf{X}) \\ \text{Maximize}: f_2(\mathbf{X}) \end{cases}. \quad (5)$$

Bounds of design variables (unit: mm):

$$\begin{cases} 0.8 \le A \le 0.9 \\ 0.7 \le B \le 0.8 \\ 0.6 \le C \le 0.7 \\ 0.55 \le D \le 0.6 \\ 45 \le E \le 50 \end{cases}, \quad (6)$$

where X is a vector of design variables. Parameters A, B, C, and D are the thickness of right circular hinges. Parameter E is the thickness of leaf hinges. The stroke and safety factor are represented as $f_1(\mathrm{X})$ and $f_2(\mathrm{X})$, respectively.

3. Proposed Modeling and Optimization Method

As designed in Figure 1, the proposed MPM platform is a monolithic architecture with three robotic legs. The translations and rotation motions of the platform are totally based on the elastic motions of the leaf hinges and right circular hinges.

Because the MPM platform is built using the concept of flexure-based mechanism, so-called compliant mechanism,

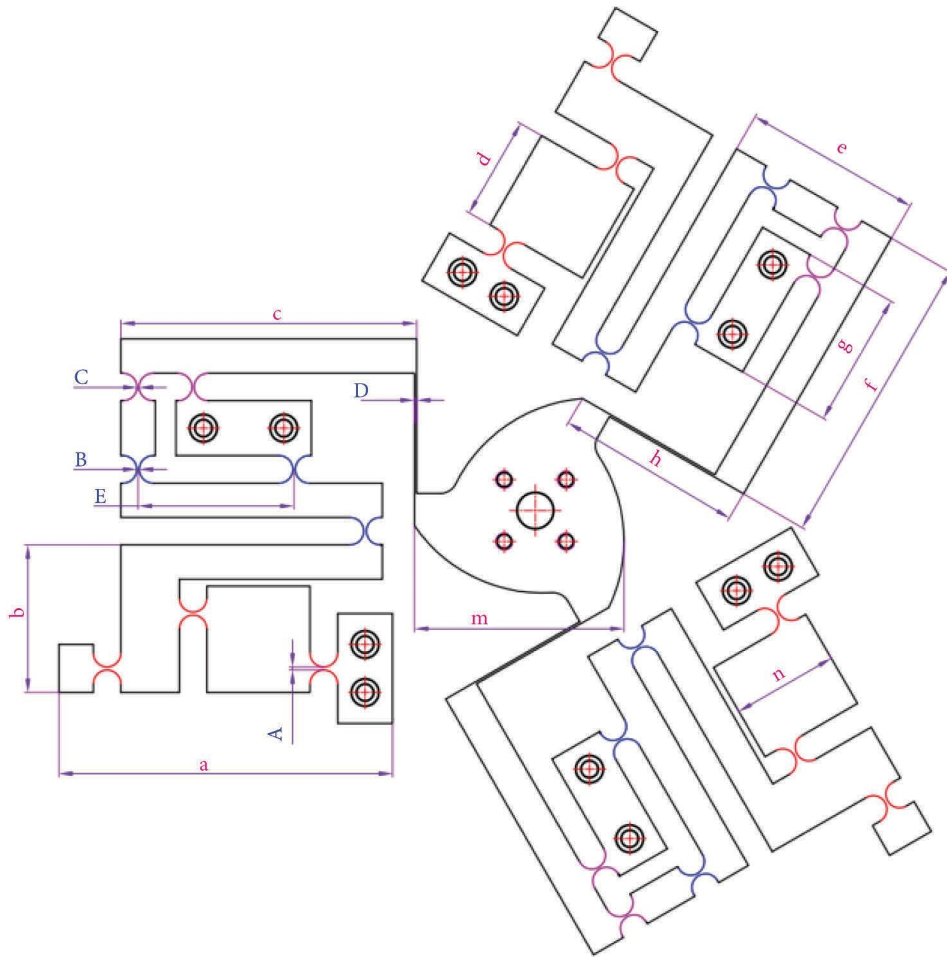

Figure 4: Mechanical scheme of proposed $XY\theta$ monolithic mechanism: (a) $XY\theta$ stage, (b) parameters.

Table 1: Dimensions of the $XY\theta$ microrobotic platform (unit: mm).

Par.	Value	Par.	Value	Par.	Value	Unit
a	97	f	86	A	$0.8 \le A \le 0.9$	mm
b	43	g	40	B	$0.7 \le B \le 0.8$	mm
c	86	h	54	C	$0.6 \le C \le 0.7$	mm
d	30	m	60	D	$0.55 \le D \le 0.6$	mm
e	52	n	32	E	$45 \le E \le 50$	mm

it inherits many excellent properties such as low weight, reduced assemble, simple fabrication, and without kinematic joints in comparison with rigid-link counterparts. Nevertheless, mathematical equations in modeling of the static behaviors of the MPM platform is difficult to exactly formulate because it has not kinematic joints. Therefore, the leaf hinges and right circular hinges are treated as virtual joints.

As a result, a modeling method based on ANN is chosen in approximating the stroke and the safety factor. In order to enhance the prediction ability of the ANN, the TLBO algorithm is employed. And then, the TLBO is extended to handle the three optimization cases of the MPM platform. The flowchart of the proposed modeling and optimization techniques is provided in Figure 9.

3.1. Simulation Technique for Microrobotic Platform. In order to collect the data of the performances of the MPM platform, the FEA implements are carried out, as seen in Figure 10. With five design variables, twenty-seven experimental samples are made.

(i) Build 3D model of the proposed MMP platform.

(ii) Design variables (A, B, C, D, and E) and output performances (stroke and safety factor) are parameterized.

(iii) Define properties of material Al 7075-T651.

(iv) Determine boundary conditions and a load/input displacement from PZT.

(v) Simulate the MPM platform by finite element method (FEM).

(vi) Collect the data.

(vii) If the data sets are not satisfied, it will return to adjust the range of variables.

3.2. ANN Optimization by TLBO. In this study, feedforward-learning ANN technique is selected to formulate the modeling of stroke and safety factor for the proposed MPM platform. Basically, ANN is operated based on human brain

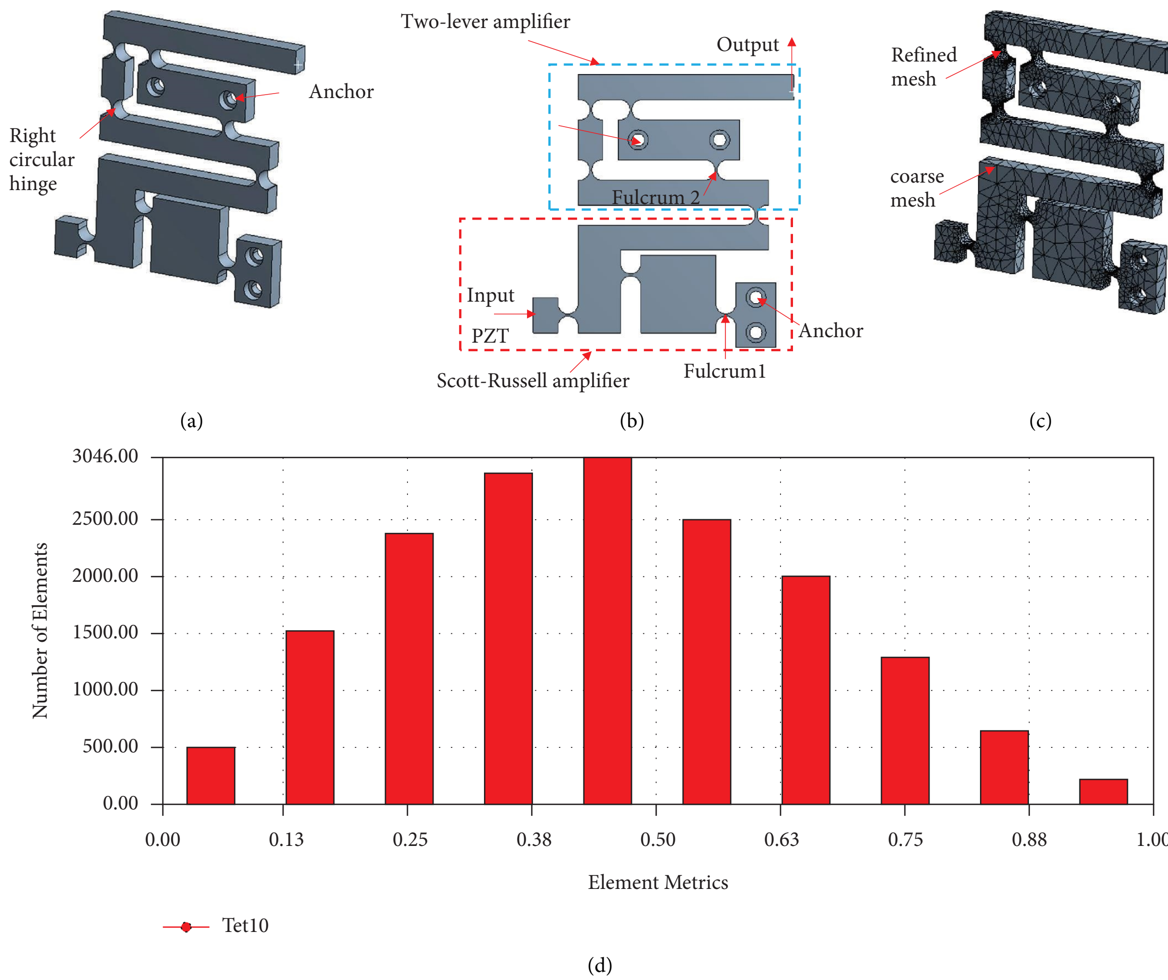

Figure 5: Proposed hybrid displacement amplifier: (a) 3D, (b) 2D, (c) meshing, (d) mesh quality.

Table 2: Results of amplification ratio of proposed HDMA.

Input (μm)	Output (μm)	Amplification ratio (μm/μm)	Stress (MPa)	Safety factor
90	1118.9	12.43	217.09	2.31
105	1305.4	12.43	253.27	1.98
125	1554.1	12.43	301.52	1.66
135	1678.4	12.43	325.64	1.54
145	1802.7	12.43	349.76	1.43

[18]. In the reasoning of ANN, the geometrical parameters and output responses of the MPM platform are embedded into the programming. An ANN programming includes three main signals such as input, hidden, and output layer. To effectively operate, the learning rate, momentum rate, bias, minimum error, and activation function should be appropriately defined. Operation of the ANN can gain a high effectiveness when it can ensure a minimal training error. This can be well done when the weight and bias are reasonably updated.

Although the ANN can build nonlinear behavior modeling but the accuracy is still strongly dependent on its controllable factors. To solve this limitation, the TLBO [19] is applied to optimize the ANN architecture. One of the most problems is how to define exactly the number of hidden nodes in hidden layer. The following equation is utilized to resolve this problem.

$$\text{Number of hidden nodes} = (2 * \text{inputs}) + \text{outputs}. \tag{7}$$

With five design variables corresponding to one output performance, the hidden layer is 11 nodes. An optimization of ANN by TLBO is provided in Figure 11.

In the optimization problem, the objective function is mean square error (MSE) which is defined as below:

$$MSE = \frac{1}{k}\sum_{i=1}^{k}\left(t_i - \widehat{t}_i\right)^2, \tag{8}$$

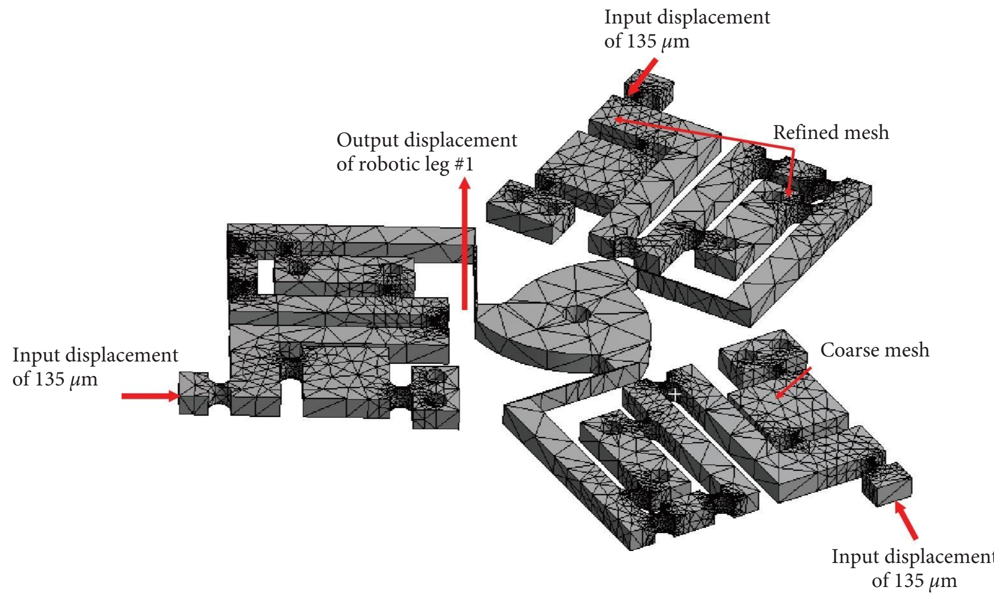

(a)

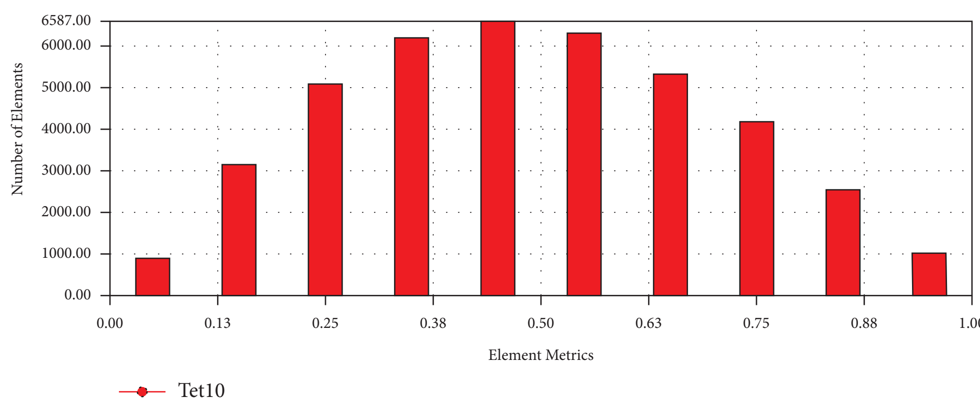

(b)

Figure 6: Simulation of the microrobotic platform: (a) boundary conditions, (b) mesh quality.

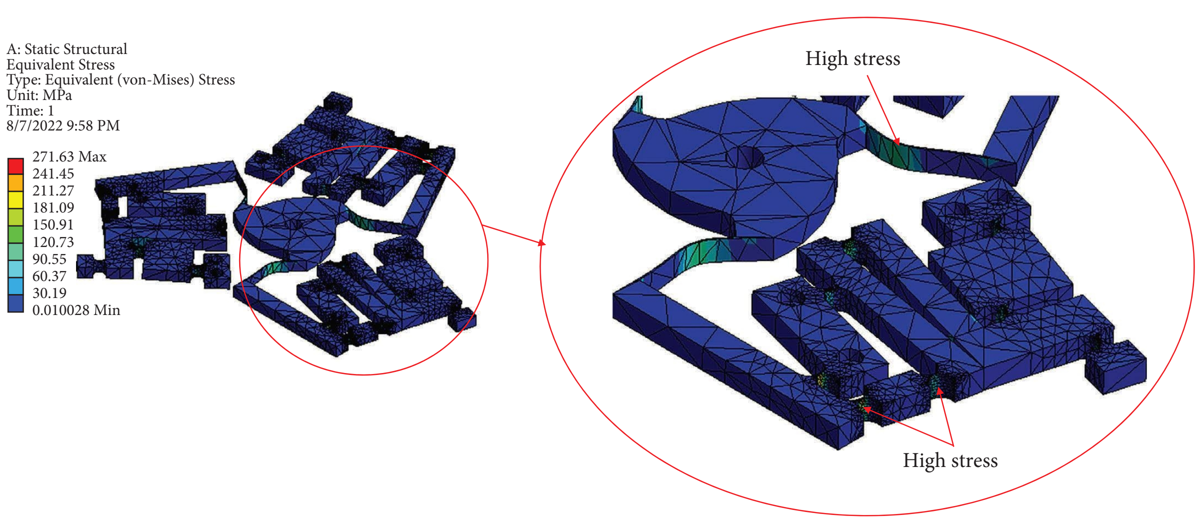

Figure 7: Stress concentration.

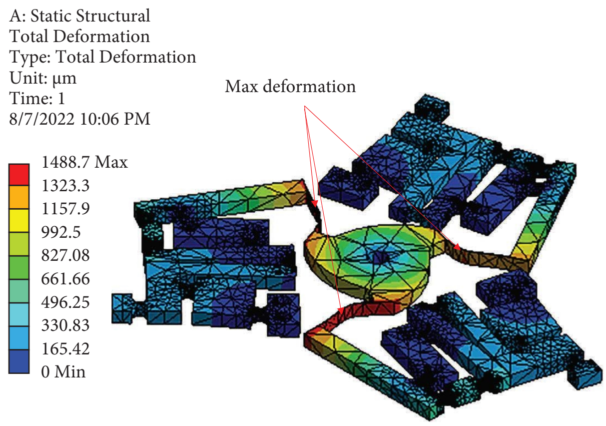

Figure 8: Deformation simulation.

Table 3: Results of static behavior.

Input (μm)	Output (μm)	Amplification ratio	Stress (MPa)	Safety factor
90	886.59	9.85	181.09	2.77
105	1034.4	9.85	211.27	2.38
125	1231.4	9.85	251.51	1.99
135	1329.9	9.85	271.63	1.85
145	1428.4	9.85	291.75	1.72

where, t is the measured target and $\hat{t}$ is the predicted target, and k is the dimension of inputs, so-called the number of data points.

Additionally, the coefficient of determination (R^2) is computed to estimate the regression model:

$$\mathrm{R}^2 = \frac{\sum_{i=1}^{k} (t_i - \bar{t})(\hat{t}_i - \bar{t})}{\sqrt{\sum_{i=1}^{k} (t_i - \bar{t})^2 \sum_{i=1}^{k} (\hat{t}_i - \bar{t})^2}}, \tag{9}$$

where t is the actual target, $\hat{t}$ is the predicted target, and $\bar{t}$ is the average target.

3.3. Optimization of Microrobotic Platform by TLBO Method. According to the TLBO algorithm, a good teacher can train a better learner. The task of teachers in a classroom is critically important [19]. The leaner is a population where a vector of design is a course vector. The two main strategies of the TLBO include teaching and learning.

3.3.1. Teaching Strategy. The teacher strategy proposes some key ideals as follows.

(i) Search the teacher with best solution from the population.

(ii) Determine the mean results of learners ($M_{j,i}$) with respect to a specific subject.

(iii) The teacher's ability affects the quality of students by following equation.

$$Dm_{j,k,i} = r_{j,i}\left(X_{j,kbest,i} - T_F M_{j,i}\right). \tag{10}$$

where, $Dm_{j,k,i}$ is the increased mean value. $X_{j,kbest,i}$ is the best learner (i.e., teacher) in jth subject. T_F is the teaching factor. $r_{j,i}$ is a random value in [0, 1]. The T_F value is either 1 or 2. The T_F value is randomly determined by the following formula:

$$T_F = \mathrm{round}\left[1 + \mathrm{rand}(0,1)\{2-1\}\right]. \tag{11}$$

After that, the existing solution is updated by the following equation in the teacher strategy.

$$X'_{j,k,i} = X_{j,k,i} + Dm_{j,k,i}, \tag{12}$$

where, $X'_{j,k,i}$ is the updated value of $X_{j,k,i}$. If the results of this phase are satisfied, and then, they are considered as inputs for the learner strategy.

3.3.2. Learning Strategy. The learners can study somethings from other students in a classroom. At any iteration i, a learner is compared with the other learners. Specifically, U and V are two learners which are compared together ($X'_{U,i} \neq X'_{V,i}$) by following formula.

$$\begin{cases} X''_{j,U,i} = X'_{j,U,i} + r_{j,i}\left(X'_{j,U,i} - X'_{j,V,i}\right), \text{if } f\left(X'_{U,i}\right) < f\left(X'_{V,i}\right) \\ X''_{j,U,i} = X'_{j,U,i} + r_{j,i}\left(X'_{j,V,i} - X'_{j,U,i}\right), \text{if } f\left(X'_{V,i}\right) < f\left(X'_{U,i}\right) \end{cases}. \tag{13}$$

$X''_{j,U,i}$ is accepted when the value of objective function is better. Flowchart of the TLBO method is given in Figure 12.

4. Results and Discussion

In this part, modeling behaviors of the MPM platform is provided. Besides, the optimization problems of the proposed platform are performed. The optimized results are validated.

Table 4: Results of dynamic behavior with input displacement of 135 μm.

No.	Mode shape	Natural frequency (Hz)
(1) z-axis translation	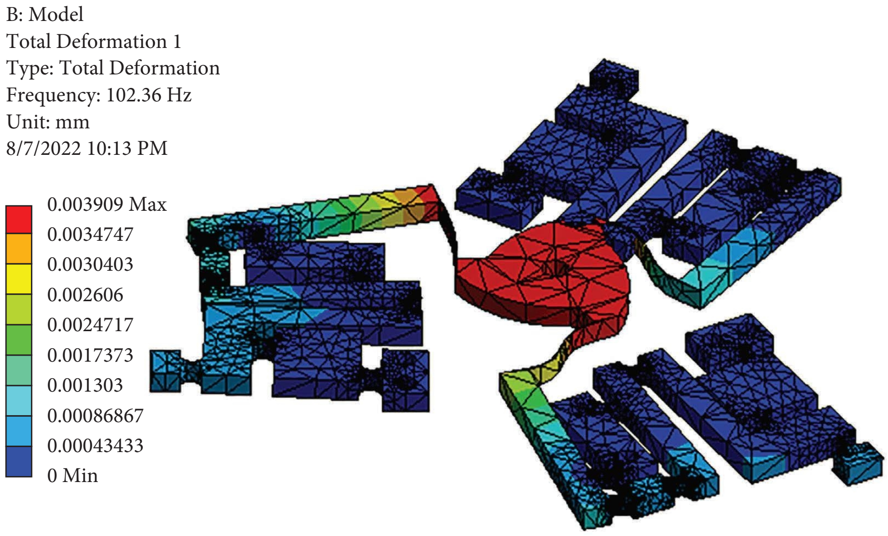	102.36
(2) x-axis translation	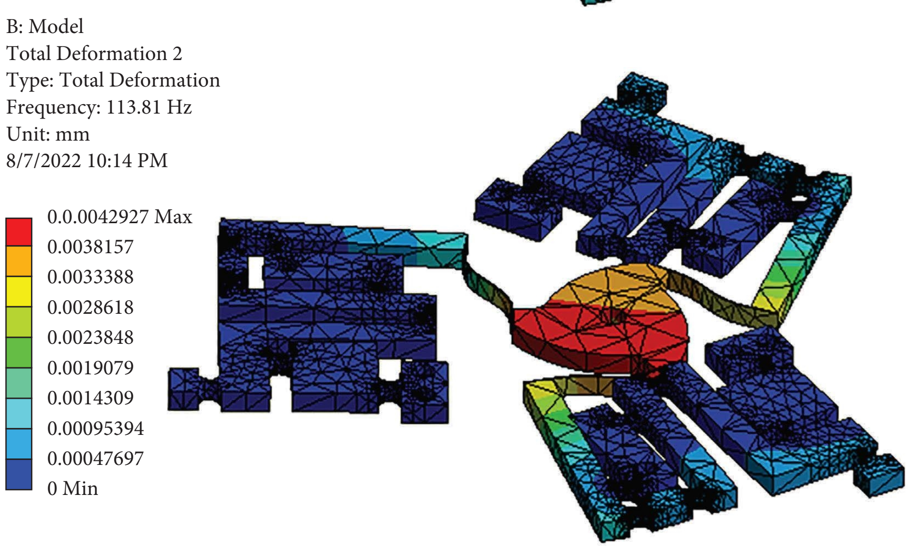	113.81
(3) z-axis translation	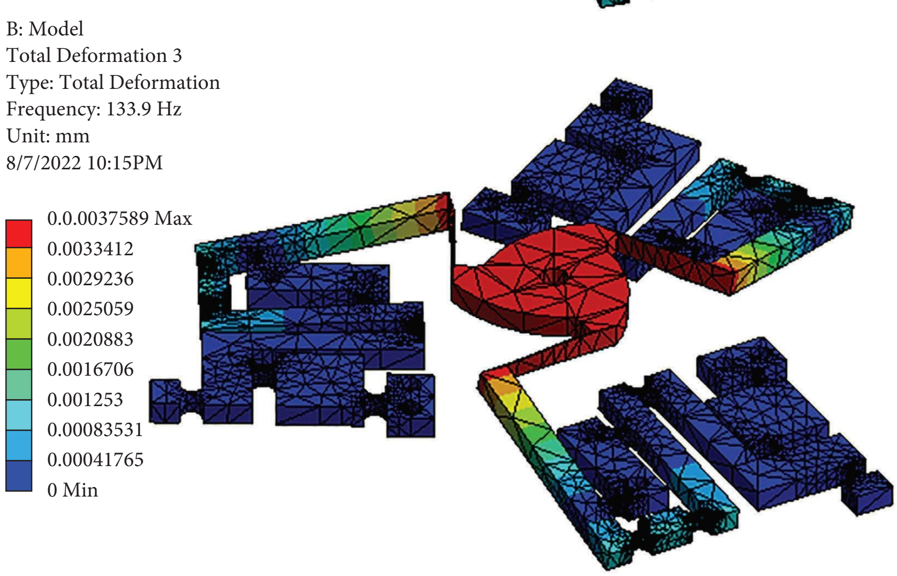	113.9

Table 4: Continued.

No.	Mode shape	Natural frequency (Hz)
(4) z-axis rotation	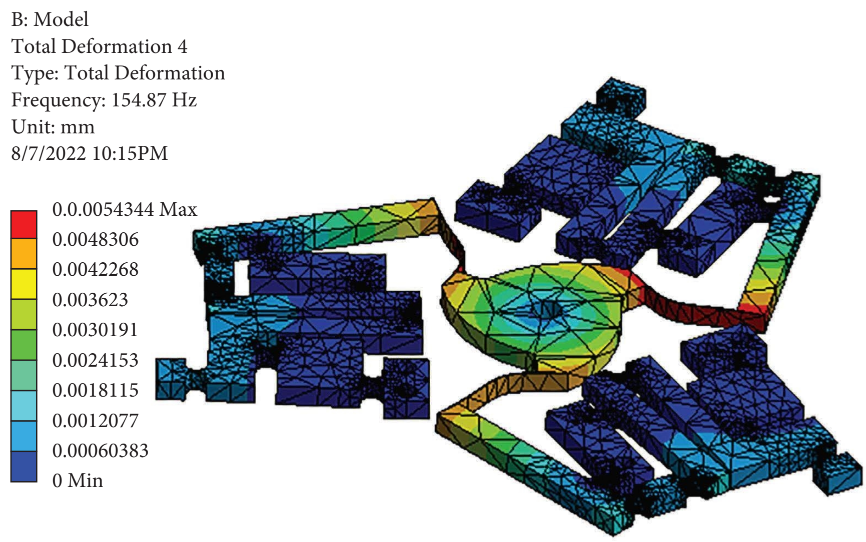	154.84

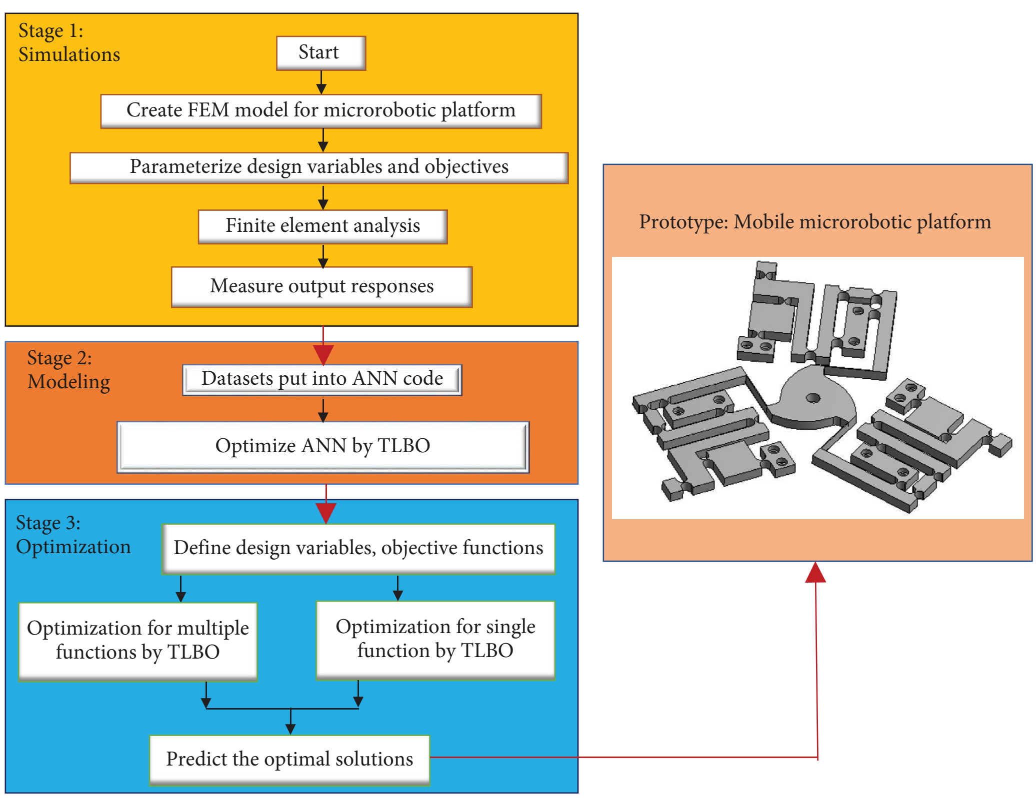

Figure 9: Flowchart of modeling and optimizing method for microrobotic platform.

4.1. Setup of Simulations and Data Collection. From Figure 5, the boundary conditions are seen. Three input displacements from three PZTs are acted simultaneously. The stroke (δ_{y1}) along the y-axis is measured. Besides, the safety factor is calculated. AL 7075-T651 is employed for the platform. The results of 27 experiments are given in Table 5.

4.2. Parametric Evaluation. To assess the associations of the geometrical parameters to the behaviors of the proposed MPM platform, analysis of variance (ANOVA) is adopted to solve this issue. The ANOVA results of stroke are given in Table 6. Moreover, the sensitive plot of whole inputs to the stroke is illustrated in Figure 13. The results indicated that

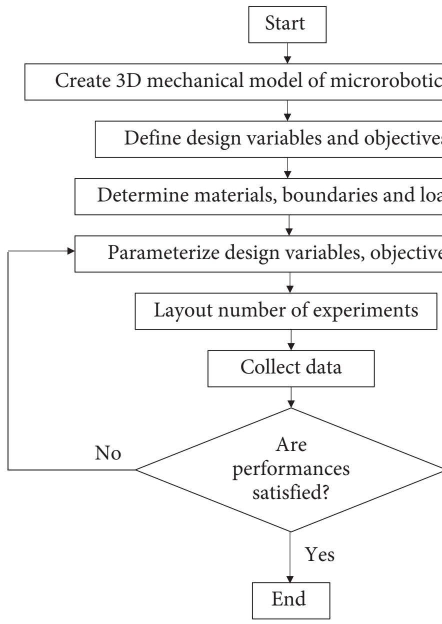

FIGURE 10: Proposed simulation scheme for microrobotic platform.

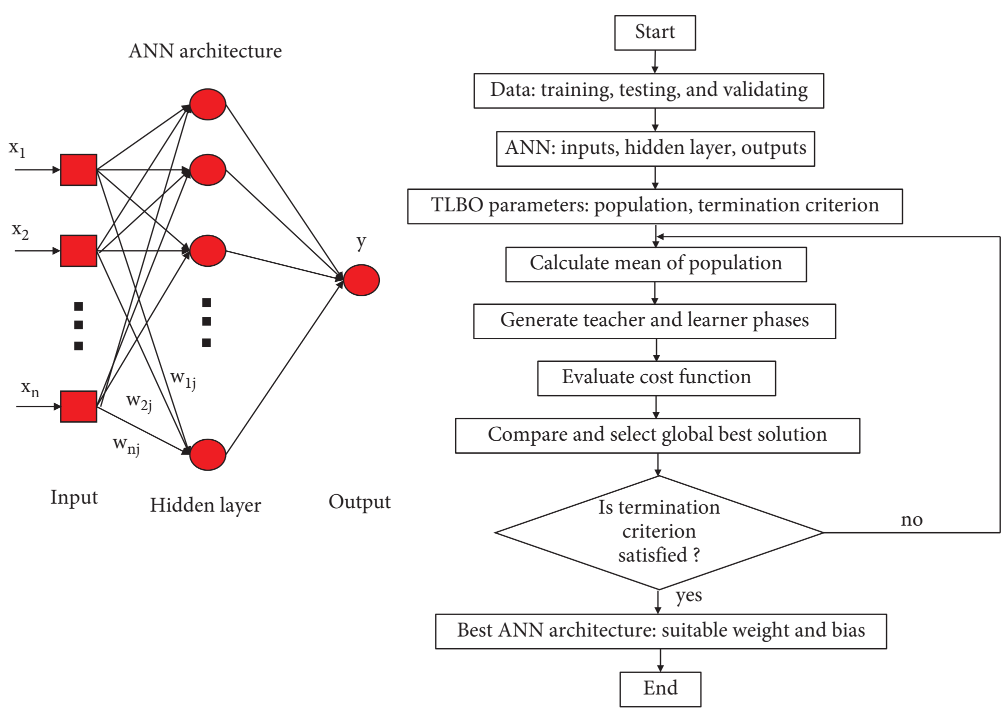

FIGURE 11: Scheme of optimization of ANN by TLBO.

the contributions of the parameters are listed as follows: C (37.65%), D (12.47%), E (7.20%), B (0.61%), and A (0.47%).

As shown in Table 7, the contributions of the input parameters on the safety factor are ordered as follows. The highest contribution is C (29.35%), A (5.78%), E (1.43%), B (1.98%), and D (0.06%), as provided in Figure 14.

4.3. Modeling Behaviors of Microrobotic Platform by ANN-Based TLBO. Modeling behaviors of the MPM platform is carried out through the ANN. To improve the effectiveness of the ANN technique, the TLBO is embedded into the ANN programming. Firstly, the collected data in Table 5 comprised of training, testing, and validating. The

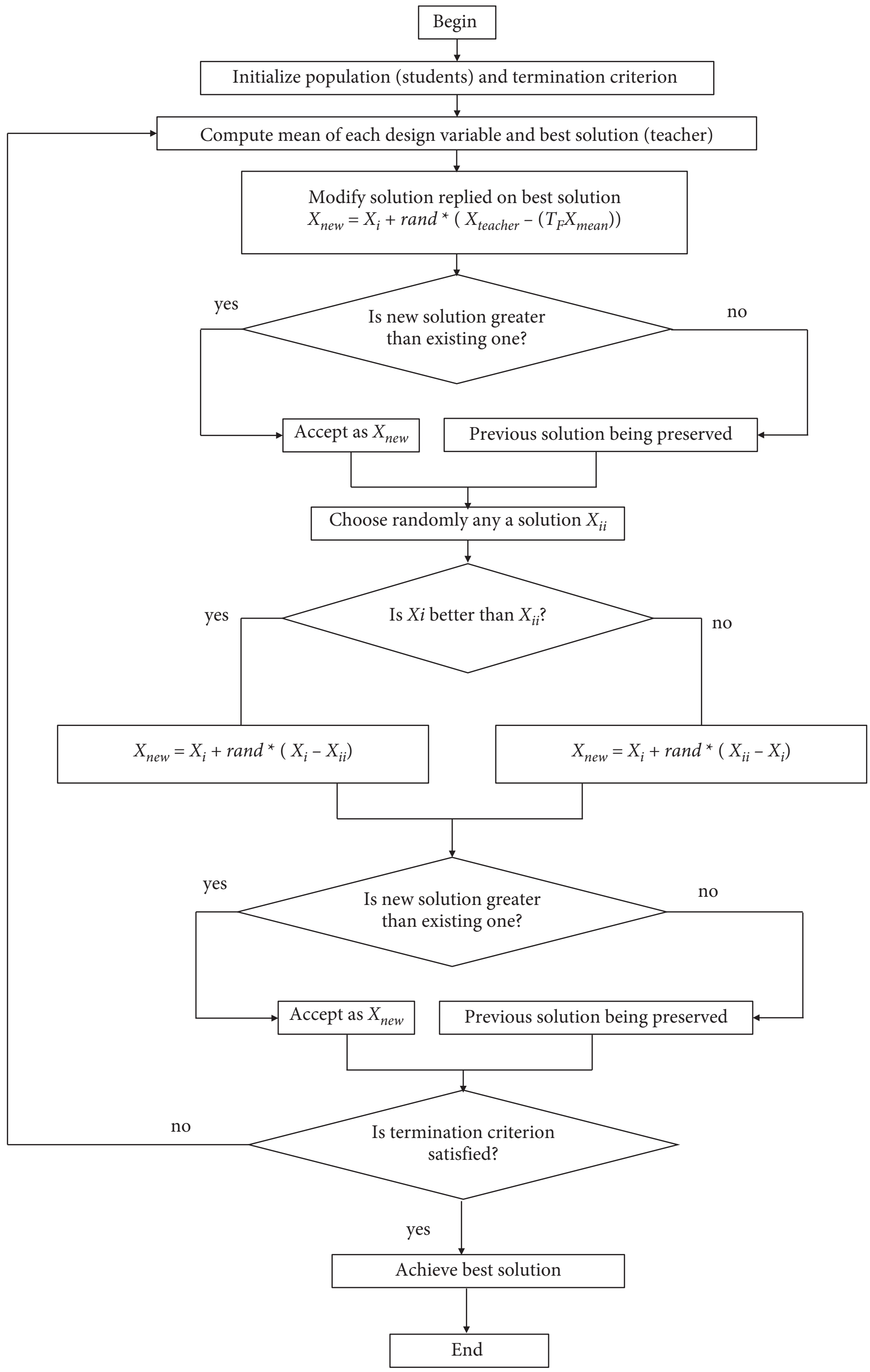

Figure 12: Flowchart of teaching-learning-based optimization method.

optimized ANN architecture can find the best weights and biases. The modeling accuracy of the optimized ANN is assessed by metric computation of the MSE and R^2.

Furthermore, the correlation coefficients (R) are also computed. The modeling results of the stroke and safety factor achieved very well with high R values, as plotted in Figures 15 and 16(a), respectively. The best performance, the prediction error, and the difference among the prediction and numerical values are provided, as seen in Figures 15, 16(c), and 16(d), respectively.

Table 5: Numerical results for the MPM platform.

No.	A (mm)	B (mm)	C (mm)	D (mm)	E (mm)	Stroke (μm)	Safety factor
1	0.85	0.75	0.65	0.6	50	1274.459	1.795
2	0.8	0.75	0.65	0.6	50	1271.977	2.216
3	0.9	0.75	0.65	0.6	50	1247.641	1.819
4	0.85	0.7	0.65	0.6	50	1270.549	2.003
5	0.85	0.8	0.65	0.6	50	1291.601	1.900
6	0.85	0.75	0.6	0.6	50	1316.365	1.747
7	0.85	0.75	0.7	0.6	50	1144.243	2.017
8	0.85	0.75	0.65	0.55	50	1355.784	1.905
9	0.85	0.75	0.65	0.65	50	1219.778	1.951
10	0.85	0.75	0.65	0.6	45	1292.106	1.945
11	0.85	0.75	0.65	0.6	55	1114.789	1.915
12	0.83	0.73	0.63	0.58	51.41	1285.452	1.896
13	0.86	0.73	0.63	0.58	48.58	1339.131	1.989
14	0.83	0.76	0.63	0.58	48.58	1350.635	1.612
15	0.86	0.76	0.63	0.58	51.41	1343.359	1.978
16	0.83	0.73	0.66	0.58	48.58	1245.309	2.223
17	0.86	0.73	0.66	0.58	51.41	1231.288	1.959
18	0.83	0.76	0.66	0.58	51.41	1359.739	2.101
19	0.86	0.76	0.66	0.58	48.58	1320.488	1.967
20	0.83	0.73	0.63	0.61	48.58	1370.22	1.806
21	0.86	0.73	0.63	0.61	51.41	1371.444	1.933
22	0.83	0.76	0.63	0.61	51.41	1362.347	1.929
23	0.86	0.76	0.63	0.61	48.58	1278.259	1.784
24	0.83	0.73	0.66	0.61	51.41	1158.641	2.032
25	0.86	0.73	0.66	0.61	48.58	1231.481	2.034
26	0.83	0.76	0.66	0.61	48.58	1190.894	2.002
27	0.86	0.76	0.66	0.61	51.41	1210.883	2.261

Table 6: Analysis of variance for the stroke.

Source	DF	Seq SS	Contribution (%)	Adj SS	Adj MS	F-value	P value
Model	20	120513	89.49	120513	6025.7	2.56	0.124
Linear	5	78626	58.39	74177	14835.4	6.29	0.022
A	1	629	0.47	402	401.5	0.17	0.694
B	1	816	0.61	538	538.3	0.23	0.650
C	1	50697	37.65	42836	42836.3	18.17	0.005
D	1	16789	12.47	22090	22089.6	9.37	0.022
E	1	9695	7.20	8915	8914.8	3.78	0.100
Square	5	11426	8.49	11673	2334.7	0.99	0.494
A*A	1	3	0.00	543	542.9	0.23	0.648
B*B	1	847	0.63	0	0.1	0.00	0.995
C*C	1	971	0.72	2371	2371.5	1.01	0.355
D*D	1	1855	1.38	125	125.0	0.05	0.826
E*E	1	7750	5.76	7236	7236.3	3.07	0.130
2-Way interaction	10	30461	22.62	30461	3046.1	1.29	0.392
A*B	1	3646	2.71	3897	3897.1	1.65	0.246
A*C	1	1382	1.03	1339	1338.9	0.57	0.480
A*D	1	6	0.00	149	148.8	0.06	0.810
A*E	1	612	0.45	654	654.0	0.28	0.617
B*C	1	5120	3.80	6498	6498.5	2.76	0.148
B*D	1	8707	6.47	7900	7900.3	3.35	0.117
B*E	1	2376	1.76	2570	2570.0	1.09	0.337
C*D	1	7492	5.56	7488	7488.1	3.18	0.125
C*E	1	1115	0.83	1103	1102.8	0.47	0.520
D*E	1	6	0.00	6	5.9	0.00	0.962
Error	6	14147	10.51	14147	2357.9		
Total	26	134661	100.00				

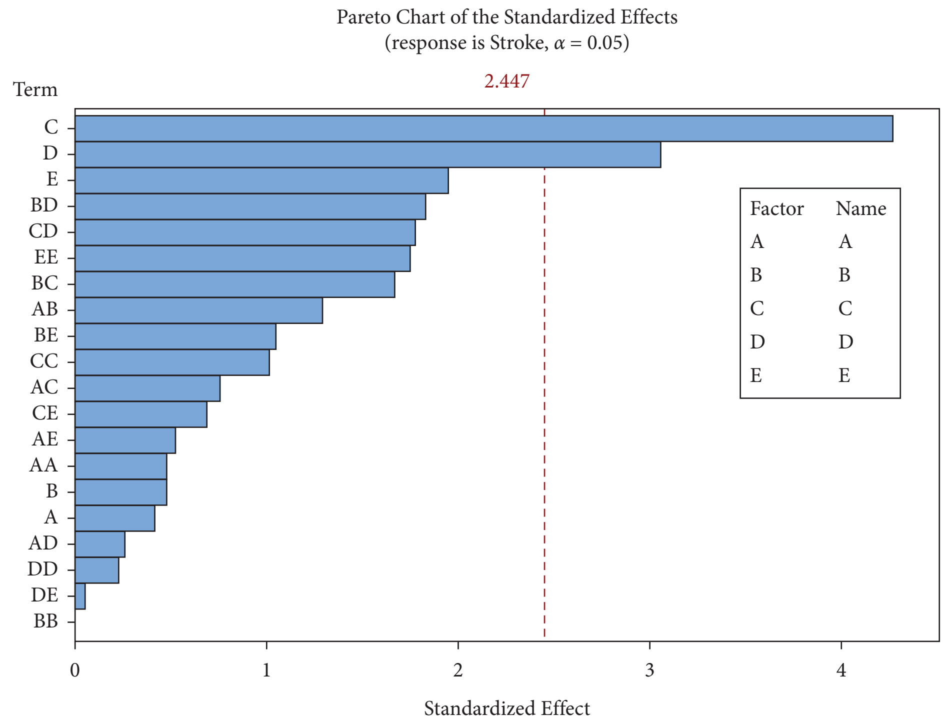

Figure 13: Sensitivity plot of design variables to the stroke.

Table 7: Analysis of variance for safety factor.

Source	DF	Seq SS	Contribution (%)	Adj SS	Adj MS	F-value	P value
Model	20	0.396108	72.62	0.396108	0.019805	0.80	0.679
Linear	5	0.210502	38.59	0.167944	0.033589	1.35	0.359
A	1	0.031505	5.78	0.041489	0.041489	1.67	0.244
B	1	0.010822	1.98	0.003362	0.003362	0.14	0.726
C	1	0.160082	29.35	0.109272	0.109272	4.39	0.081
D	1	0.000303	0.06	0.001510	0.001510	0.06	0.814
E	1	0.007789	1.43	0.010727	0.010727	0.43	0.536
Square	5	0.020878	3.83	0.020510	0.004102	0.16	0.967
A*A	1	0.006593	1.21	0.001006	0.001006	0.04	0.847
B*B	1	0.000844	0.15	0.000710	0.000710	0.03	0.871
C*C	1	0.010358	1.90	0.012192	0.012192	0.49	0.510
D*D	1	0.000886	0.16	0.002319	0.002319	0.09	0.770
E*E	1	0.002196	0.40	0.002143	0.002143	0.09	0.779
2-Way interaction	10	0.164728	30.20	0.164728	0.016473	0.66	0.731
A*B	1	0.001177	0.22	0.001342	0.001342	0.05	0.824
A*C	1	0.056306	10.32	0.056556	0.056556	2.27	0.182
A*D	1	0.000000	0.00	0.000038	0.000038	0.00	0.970
A*E	1	0.000713	0.13	0.001278	0.001278	0.05	0.828
B*C	1	0.004343	0.80	0.003475	0.003475	0.14	0.721
B*D	1	0.018617	3.41	0.018649	0.018649	0.75	0.420
B*E	1	0.057861	10.61	0.060386	0.060386	2.43	0.170
C*D	1	0.000085	0.02	0.000084	0.000084	0.00	0.955
C*E	1	0.022801	4.18	0.023640	0.023640	0.95	0.367
D*E	1	0.002825	0.52	0.002825	0.002825	0.11	0.748
Error	6	0.149333	27.38	0.149333	0.024889		
Total	26	0.545441	100.00				

As depicted in Figures 15 and 16, the proposed artificial intelligent technique had better performances than those achieved from the linear regression.

4.4. Parameter Optimization. In this part, the TLBO algorithm is initialized with a population of 50 and iterations of 5000. The optimization programming is implemented

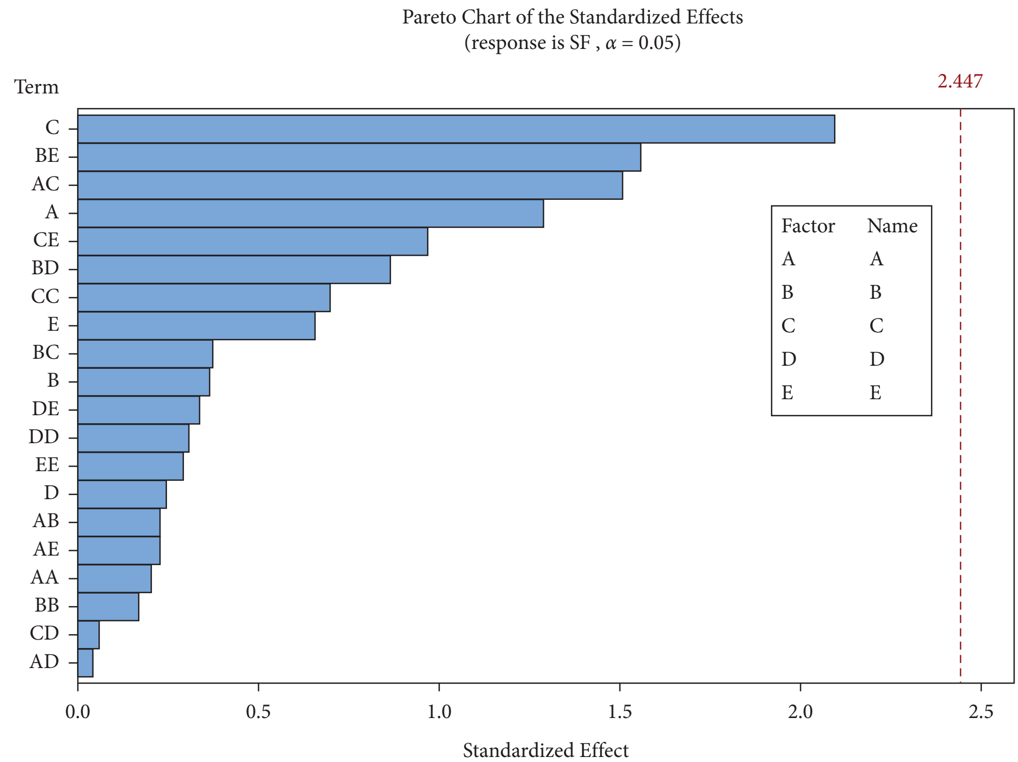

FIGURE 14: Sensitivity plot of design variables to the safety factor.

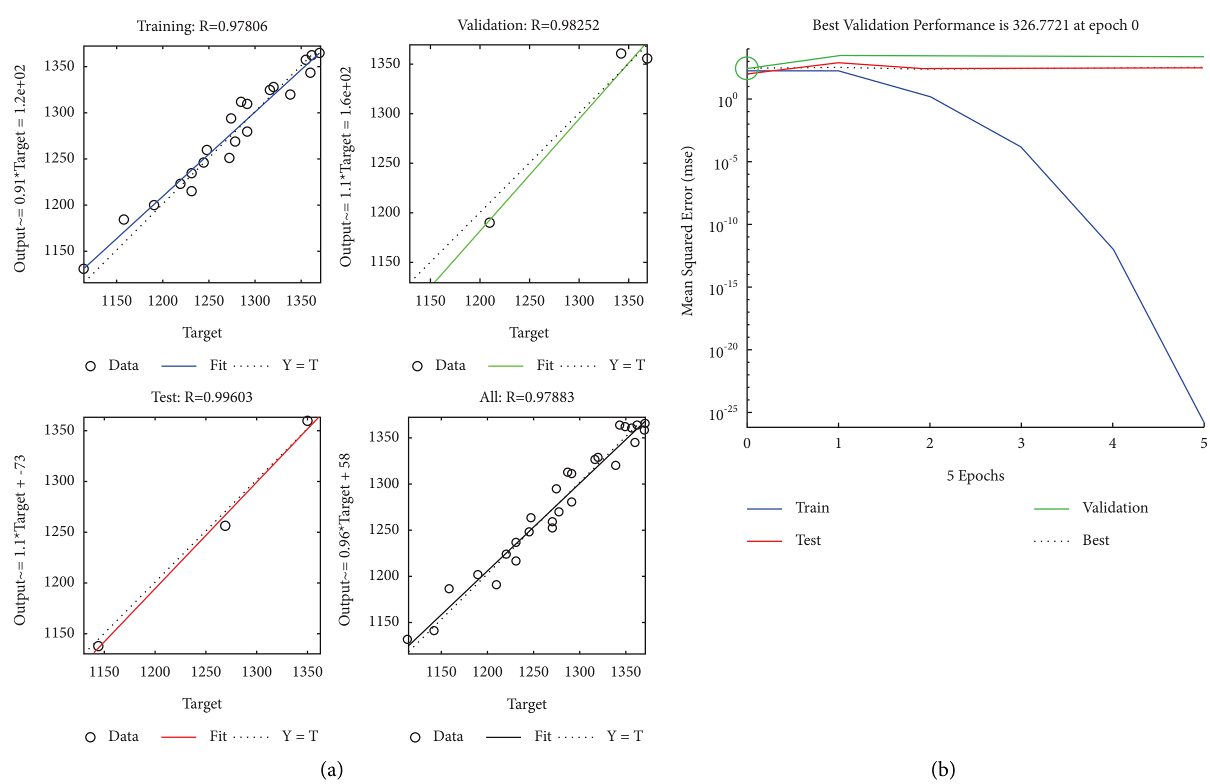

FIGURE 15: Continued.

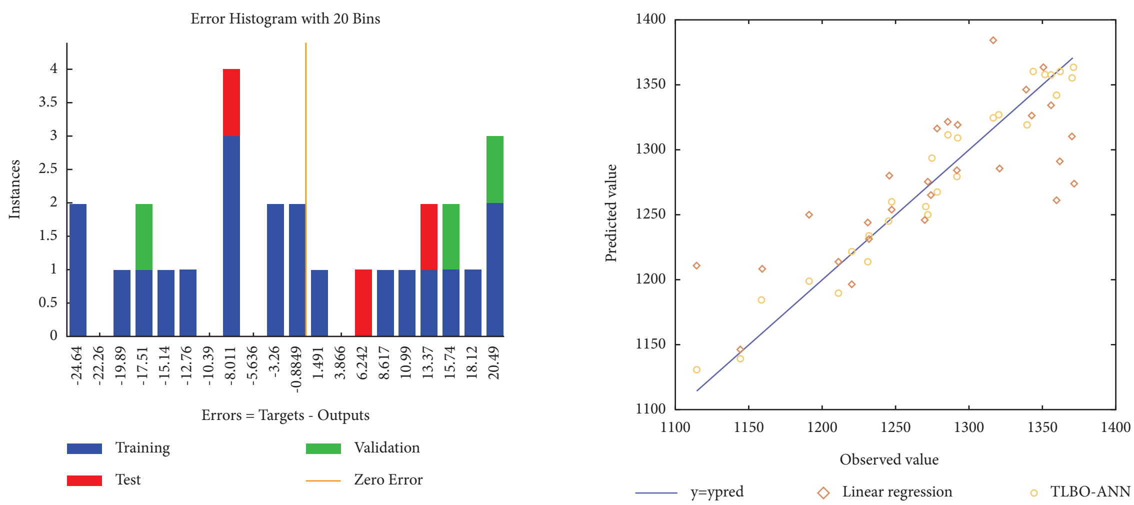

(c) (d)

Figure 15: Modeling for stroke by ANN-combined TLBO method: (a) training, (b) performance, (c) error, (d) predicted vs measured value.

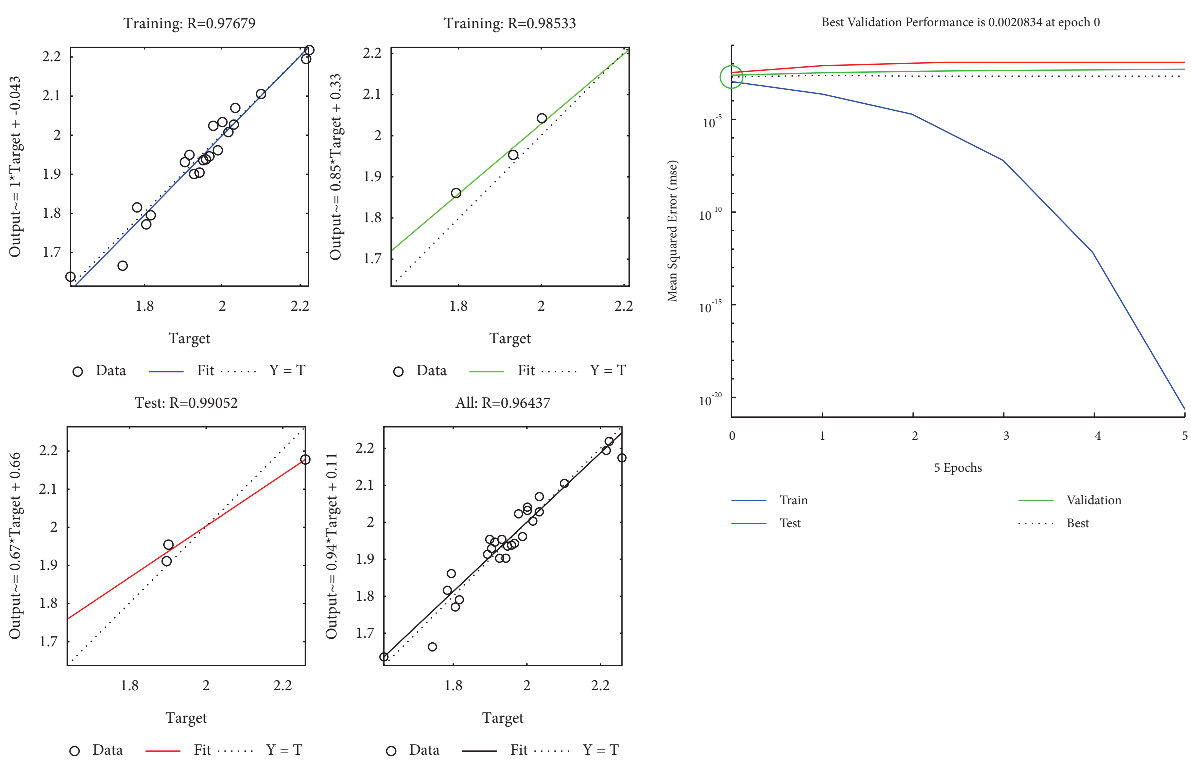

(a) (b)

Figure 16: Continued.

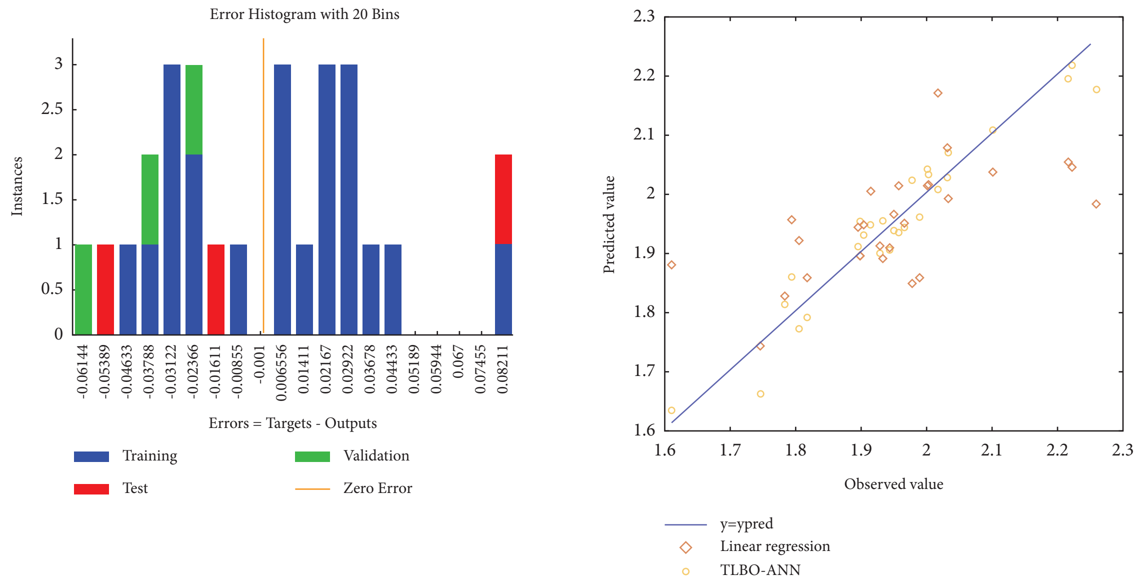

(c) (d)

FIGURE 16: Modeling for safety factor by ANN-combined TLBO method: (a) training, (b) performance, (c) error, (d) predicted vs measured value.

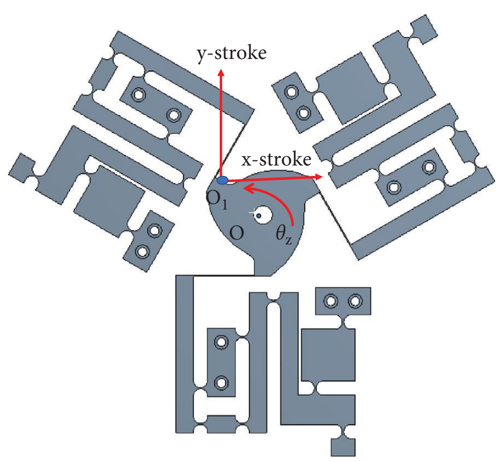

FIGURE 17: Measurement of rotation angle of the microrobotic platform.

MATLAB R2019 environment. The optimized results for the three case studies are provided in Table 6. From Figure 17, the rotation angle (θ_z) around the O point of the proposed MPM platform is measured by FEA ANSYS software. From Table 8, the y-stroke is the displacement along the y-axis at O_1 point. The y-stroke is the optimized displacement which is predicted from the proposed metaheuristic-intelligent method (ANN-TLBO). The x-stroke is the displacement along the x-axis at O_1 point. The x-stroke, the stress and the rotation angle are calculated from the FEA ANSYS software.

From the achieved results of Table 8, it revealed that the optimized strokes in the y-axis of the MPM platform can obtain 1555.6763 μm, 1300.6 μm, and 1568 μm for case #1, case #2, and case #3, respectively. Besides, the x-axis strokes of the platform are 266.4 μm, 735.55 μm, and 714 μm for case #1, case #2, and case #3, respectively. The safety factor of the platform is over 1.5. Meanwhile, the stress appeared in three case studies is always lower than the yield stress (503 MPa) of AL 7075-T651. This guarantees a long working strength for the platform. The stress is calculated by the following equation.

$$S = \frac{S_{\text{yield}}}{SF}, \tag{14}$$

where, S represents the stress of the MPM platform. S_{yield} is the yield stress of AL 7075-T651. SF is the safety factor.

Based on the output stroke of the proposed MPM platform, the displacement amplification ratio can be calculated by following formula.

$$A_R = \frac{O_S}{I_S}, \tag{15}$$

Table 8: Optimum results for three case studies.

	Cases	Optimal solutions (mm)	y-stroke (μm)	x-stroke (μm)	Safety factor	Stress (MPa)	Rotation angle (degree)
TLBO for single-objective problems	Case 1	$A = 0.9$, $B = 0.8$, $C = 0.6$, $D = 0.6$, $E = 50$	1558.6763	266.4	1.58	318.35	1.85
	Case 2	$A = 0.87$, $B = 0.7$, $C = 0.6$, $D = 0.55$, $E = 49$	1300.6	735.55	2.33	215.87	1.97
TLBO for multi-objective problems	Cases	Optimal solutions (mm)	Stroke (μm)	x-stroke (μm)	Safety factor	Stress (MPa)	Rotation angle (degree)
	Case 3	$A = 0.89$, $B = 7.97$, $C = 0.6$, $D = 0.55$, $E = 45$	1568.1	714	2.04	246.56	2.26

Table 9: Validation results.

Case study	Method	Performances	
		y-stroke (μm)	Safety factor
Case 1	Proposed method	1558.6763	1.58
	FEA results	1432.2	1.47
Error (%)		8.8	7.48
Case 2	Proposed method	1300.6	2.3
	FEA results	1368.7	2.2
Error (%)		4.97	4.54
Case 3	Proposed method	1568.1	2.04
	FEA results	1689.8	2.17
Error (%)		7.2	5.9

where, A_R is the displacement amplification ratio. The O_S and I_S note the output y-stroke and input stroke.

By using equation (15), the A_R values are about 11.54 for case study #1, 9.63 for case study #2, and 11.61 for case study #3.

4.5. Validations of Optimized Results. By using the optimized design parameters, the prototypes are built in Inventor software, and then, the simulations are performed to verify the optimized results. As given in Table 9, the errors between the proposed method and the simulation method are under 9%. The proposed method is reliable optimization technique in modeling and optimizing the MPM platform.

5. Conclusions

This article has presented an optimized design method for the mobile microrobotic platform. The proposed MPM platform was built via using two combined modules, including the hybrid displacement amplification mechanism and leaf hinges. The developed HDAM was created by combination of Scott–Russell mechanism and two-double lever amplification mechanism. The new proposed HDAM amplifier could allow a large amplification ratio. With such a high amplification value, it ensured a large output stroke for the MPM platform. The developed MPM platform was able to be employed for locating the sample in the polishing robot system. The platform could achieve three motions, including two translations and one rotation.

In modeling the stroke and safety factor of the MPM platform, the ANN was used in combination with the TLBO method. By using the TLBO, the ANN architecture was optimized to a better approximation. And then, three optimized case studies were studied by the TLBO to improve the stroke and safety factor. Moreover, the case studies also demonstrated the effectiveness of the methodology. In this study, the FEM data was combined with ANN, TLBO for modeling process. The results of this paper could be listed as follows.

The modeling results from the TLBO-based ANN were well established. The metrics were relatively good with the values of R and R^2 being near 1 while the values of MSE were very small.

The established intelligent predictors were better than the linear regression. The predicted values from the TLBO-ANN were close to the measured values.

In case study #1, the optimized platform could operate with the y-axis stroke over 1558.6763 μm and a safety factor of 1.58.

In case study #2, the optimized platform could achieve a large y-axis of 1300 μm and a safety factor of 2.3.

In case study #3, the optimized platform could displace a large y-axis of 1568.1 μm and a safety factor of 2.04.

In summary, the proposed MPM platform could achieve a max-y stroke of 1568.1 μm, max-x stroke of 735.55 μm, and max-θ rotation angle of 2.26 degrees.

The stress of three cases were still lower than the yield stress of Al 7075-T651.

The proposed MPM platform could achieve a high displacement amplification ratio at least of 9.

In upcoming study, the real prototypes will be manufactured by WEDM. The physical verifications will be carried out. The polishing experiments will be conducted.

Data Availability

The data used to support the findings of this study are included within the article.

Conflicts of Interest

The authors declare that they have no conflicts of interest.

Acknowledgments

This work belongs to the project grant no: T2021-11TĐ and was funded by Ho Chi Minh City University of Technology and Education, Vietnam.

References

[1] G. Chen and F. Ma, "Kinetostatic modeling of fully compliant bistable mechanisms using timoshenko beam constraint model," *Journal of Mechanical Design*, vol. 137, no. 2, pp. 1–10, 2015.

[2] N. Le Chau, N. T. Tran, and T. P. Dao, "A multi-response optimal design of bistable compliant mechanism using efficient approach of desirability, fuzzy logic, ANFIS and LAPO algorithm," *Applied Soft Computing*, vol. 94, Article ID 106486, 2020.

[3] L. Mingming, D. Zhao, J. Lin, X. Zhou, B. Chen, and H. Wang, "Design and analysis of a novel piezoelectrically actuated vibration assisted rotation cutting system," *Smart Materials and Structures*, vol. 27, no. 9, pp. 1–9, Article ID 095020, 2018.

[4] D. N. Nguyen, N. L. Ho, T.-P. Dao, and N. Le Chau, "Multi-objective optimization design for a sand crab-inspired compliant microgripper," *Microsystem Technologies*, vol. 25, no. 10, pp. 3991–4009, 2019.

[5] X. Ma, A. Wilson, C. D. Rahn, and S. Trolier-McKinstry, "Efficient energy harvesting using piezoelectric compliant mechanisms: theory and experiment," *Journal of Vibration and Acoustics*, vol. 138, no. 2, pp. 1–9, 2016.

[6] M. L. Culpepper and G. Anderson, "Design of a low-cost nano-manipulator which utilizes a monolithic, spatial compliant mechanism," *Precision Engineering*, vol. 28, no. 4, pp. 469–482, 2004.

[7] L. U. Odhner and A. M. Dollar, "The smooth curvature model: an efficient representation of Euler-Bernoulli flexures as robot joints," *IEEE Transactions on Robotics*, vol. 28, no. 4, pp. 761–772, 2012.

[8] R. Wang and X. Zhang, "Preload characteristics identification of the piezoelectric-actuated 1-DOF compliant nano-positioning platform," *Frontiers of Mechanical Engineering*, vol. 10, no. 1, pp. 20–36, 2015.

[9] F. Wang, X. Zhao, Z. Huo et al., "A 2-DOF nano-positioning scanner with novel compound decoupling-guiding mechanism," *Mechanism and Machine Theory*, vol. 155, Article ID 104066, 2021.

[10] L. Clark, B. Shirinzadeh, Y. Tian, and B. Yao, "Development of a passive compliant mechanism for measurement of micro/nanoscale planar 3-DOF motions," *IEEE*, vol. 21, no. 3, pp. 1222–1232, 2016.

[11] S. Iqbal and A. Malik, "A review on MEMS based micro displacement amplification mechanisms," *Sensors and Actuators A: Physical*, vol. 300, Article ID 111666, 2019.

[12] H. Wang and X. Zhang, "Input coupling analysis and optimal design of a 3-DOF compliant micro-positioning stage," *Mechanism and Machine Theory*, vol. 43, no. 4, pp. 400–410, 2008.

[13] M. T. Pham, T. J. Teo, S. H. Yeo, P. Wang, and M. L. S. Nai, "A 3-D printed Ti-6Al-4V 3-DOF compliant parallel mechanism for high precision manipulation," *IEEE*, vol. 22, no. 5, pp. 2359–2368, 2017.

[14] Y. Li and Z. Wu, "Design, analysis and simulation of a novel 3-DOF translational micromanipulator based on the PRB model," *Mechanism and Machine Theory*, vol. 100, pp. 235–258, 2016.

[15] U. Bhagat, B. Shirinzadeh, L. Clark et al., "Design and analysis of a novel flexure-based 3-DOF mechanism," *Mechanism and Machine Theory*, vol. 74, pp. 173–187, 2014.

[16] W. L. Zhu, Z. Zhu, S. To, Q. Liu, B. F. Ju, and X. Zhou, "Redundantly piezo-actuated XYθ z compliant mechanism for nano-positioning featuring simple kinematics, bi-directional motion and enlarged workspace," *Smart Materials and Structures*, vol. 25, no. 12, Article ID 125002, 2016.

[17] D. H. Chao, R. Liu, Y. M. Wu, L. Shi, and G. H. Zong, "Manufacturing error analysis of compliant 3-DOF microrobot," *Frontiers of Mechanical Engineering in China*, vol. 1, no. 3, pp. 299–304, 2006.

[18] G. Villarrubia, F. Juan, D. Paz, P. Chamoso, and F. De la Prieta, "Artificial neural networks used in optimization problems," *Neurocomputing*, vol. 272, pp. 10–16, 2018.

[19] R. V. Rao, V. J. Savsani, and J. Balic, "Teaching-learning-based optimization algorithm for unconstrained and constrained real-parameter optimization problems," *Engineering Optimization*, vol. 44, no. 12, pp. 1447–1462, 2012.